JOURNAL OF SPACECRAFT AND ROCKETS
Vol. 31, No. 5, September–October 1994

Examining the Accuracy of Space Shuttle Support Loads Using Probabilistic Analysis Techniques

J. A. Richardson*
University of Alabama, Tuscaloosa, Alabama 35487
and
J. S. Townsend†
NASA Marshall Space Flight Center, Huntsville, Alabama 35812

To understand unexpectedly erratic load measurements in the launch pad supports for the Space Shuttle, the sensitivities of the load cells in the supports were analyzed using simple probabilistic techniques. NASA engineers use the loads in the Shuttle's supports to calculate critical stresses in the Shuttle vehicle just before liftoff. The support loads are measured with "load cells," which actually are structural components of the mobile launch platform that have been instrumented with strain gauges. Although these load cells adequately measure vertical loads, horizontal load measurements have been erratic. Load measurements were simulated in this study using Monte Carlo simulation procedures. The simulation studies showed that the support loads are sensitive to small deviations in strain and calibration. In their current configuration, the load cells will not measure loads with sufficient accuracy to reliably calculate stresses in the Shuttle vehicle.

Nomenclature

A = matrix of calibration constants
C = reduced calibration matrix
Px = vertical holddown post load in x direction
Py = horizontal holddown post load in y direction
Pz = horizontal holddown post load in z direction

Introduction

History

THE United States Space Transportation System (Space Shuttle) is an extremely complex system and demands rigorous engineering performance. For these reasons, as well as for safety concerns, it is important that engineer's can accurately quantify loads on the Shuttle vehicle as well as load uncertainties. Typically, loads are determined from engineering analyses and testing, with loads verification requiring special instrumentation of flight hardware.

The reaction forces at the Shuttle vehicle, mobile launch platform (MLP) interface are considered in this study. A sketch of the liftoff configuration is given in Fig. 1. When positioned on the launch pad, the Space Shuttle is supported by eight posts, termed holddown posts (HDPs), which extend up from the MLP and attach to the aft skirts of the solid rocket boosters (SRBs). All shuttle external loading, such as main engine thrust, gravity, and wind, must react back to the ground through these interfaces. Knowledge of these loads defines the design or limit load criteria of the SRB support skirt and the liftoff loads and dynamics that drive the shuttle primary structure and payload. The critical loads on the skirt occur during the approximately 7-s time period immediately prior to liftoff, when the Space Shuttle main engines (SSMEs) are building up to maximum thrust. During a 1988 structural qualification test of a "modified" aft skirt, skirt post/skin welds failed at loads 1.28 times the critical loads. Because the desired factor of safety for the aft skirt was 1.40, and because SRB/MLP interface reaction loads verification has been a long-time engineering objective, NASA decided to measure the actual skirt loads during the SSME buildup phase of launch.

Commercially available load cells were not practical because of configuration constraints and the extremely large loads on the HDPs. Therefore, the HDPs themselves were instrumented with strain gauges and load calibrated, essentially making each HDP into a unique load cell. However, the HDPs were designed to be HDPs, not load cells. Designing the instrumentation for the posts was difficult because the posts were unsymmetrical and very stiff (which meant very small strains). All load-cell configuration decisions were based upon experimental-trial-and-error testing of a multistrain gauged HDP. In another study, the authors used a simplified model of the HDP load measurement system to study the effect of load measurement accuracy of several factors, including load point deviations, gauge heights, and HDP geometry.[1]

Load Cell Configuration

A close-up view of a typical HDP/aft-skirt interface is shown in Fig. 1. The structural components that make up the interface are the skirt foot (post), the skirt shoe, the epon shim, the spherical bearing, and the MLP HDP. Note also, that a pretensioned holddown stud is used to sandwich these components together. Although the load path is not simple, all loads must react through the MLP post, making it the prime candidate for the structural load cell. Figure 2 shows a photograph of a typical HDP mounted to the MLP at Kennedy Space Center.

The strain gauge transducers for the HDP load cell are located on the inside of the post. Eight strain gauge clusters are positioned in a single ring around the inner circumference of the HDP at a distance of about 28 in. from the top of the post. Each cluster consists of four axial gauges arranged to compensate for temperature and Poisson effects and to amplify output sensitivity. Shear gauge transducers are also positioned on the posts, but because of extremely low output, these gauges have proved to be of little practical use. As mentioned in the introduction, the current HDP load cell configuration was based on findings from experimental testing. At that time, the frictional moment constraint was assumed to be a second-order effect and was ignored (the moment was assumed to be zero at the top of the post). Additional testing, however, indicated that the moment effects are not negligible. Recently, a new post load cell has been designed, tested, and flight implemented to measure both shear and moment loads. The accuracy of this "improved" load cell is also questionable.

Typical HDP load histories from eight flights are shown in Fig. 3. As seen in the figure, the vertical (x direction) loads do not deviate

Received Jan. 29, 1993; presented as Paper 93-1107 at the AIAA/AHS/ASEE Aerospace Design Conference, Irvine, CA, Feb. 16–19, 1993; revision received Aug. 30, 1993; accepted for publication Sept. 3, 1993.

*Assistant Professor, Civil Engineering Department.
†Aerospace Engineer, Structures and Dynamics Laboratory.

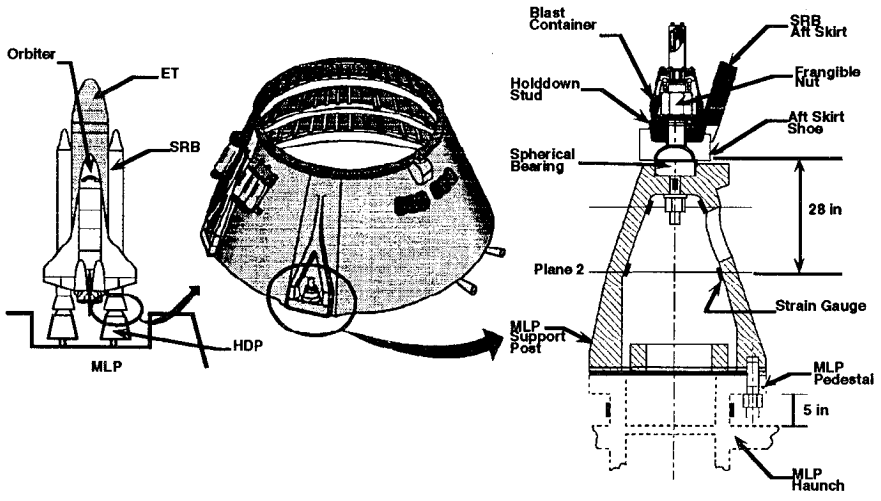

Fig. 1 SRB aft-skirt MLP interface.

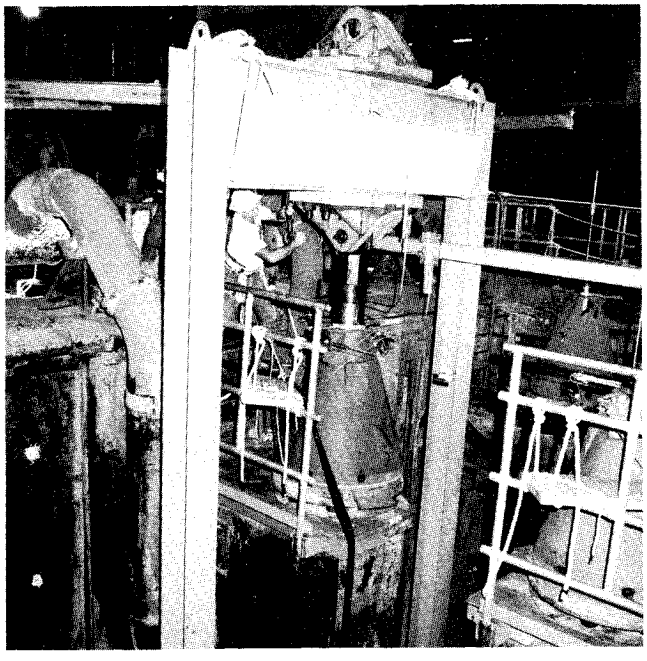

Fig. 2 HDP mounted to MLP.

much, in terms of percentage, from flight to flight. The horizontal loads, however, deviate significantly from flight to flight. This scatter in data may represent actual deviations in the HDP loads from flight to flight, or they may be due to measurement error. The z-direction loads do not satisfy equilibrium checks, however, indicating that the z load variation is due (at least partly) to measurement error.

A two-step procedure is followed to calculate stresses in the aft skirt from measured HDP strains. In this procedure, diagrammed in Fig. 4, the HDP strains are multiplied by a calibration matrix to yield HDP loads. The HDP loads are then multiplied by aft-skirt stress indicator equations to yield the aft-skirt stresses. A HDP is calibrated by removing if from the MLP and bolting it to a test stand. Controlled loads are then applied to the HDP, and the resulting strains are measured. The measured strains and loads are used to form a matrix of calibration constants for that post.

The effect of strain measurement errors and calibration constant errors on the accuracy of the HDP load measurements is examined in the next section. The x loads are shown to be the most sensitive (have the largest standard deviation) to strain measurement and calibration constant errors in an absolute sense. However, the z loads are the most sensitive in a relative sense (largest standard deviation/mean), which agrees with the actual load histories shown in Fig. 3. The deviation in HDP loads caused by strain measurement and calibration constant errors seriously affects the accuracy of the predicted aft-skirt stresses, as shown in the following section.

Accuracy of HDP Load Measurements

A simple probabilistic analysis technique, the Monte Carlo simulation, was used to investigate the effect of known sources of error on the HDP load measurements. A schematic diagram of the procedure for investigating the effects of strain measurement errors is shown in Fig. 5. Each of the eight strain measurements was assumed to vary about its mean within a range of $\pm$ deviation. This deviation represented the difference or error between the true HDP strains and the measured HDP strains. Because no actual data on the HDP strain measurement errors were available, these errors were modeled with the simplest probability distribution: the uniform distribution. In a uniform distribution, the values have an equal probability of occurrence with the range: (mean $-$ deviation) to (mean $+$ deviation).

A set of three HDP loads (Px, Py and Pz in Fig. 5) was calculated by drawing a strain measurement at random from each of the eight strain probability distributions and multiplying by the calibration matrix. This procedure was repeated 1000 times to produce the HDP-load probability distributions. The HDP-load distributions resembled bell-shaped or normal probability distributions. The measure of dispersion for these distributions is the standard deviation. The standard deviation can be normalized by dividing by the mean of the distribution to yield the coefficient of variation (COV).

Effect of Strain Variations on HDP Loads

Because the peak stresses in the aft skirt occur when the HDP loads are at the their peak values, (approximately 1.2 s before separation in Fig. 3), the measured strains from a typical flight at 1.2 s before separation were used as the mean strains for the strain distributions. The mean strains and mean loads used for the simulation are shown in Table 1. As already mentioned, no data on the actual strain measurement errors were available. A practical lower bound on strain measurement errors is ± 5 microstrains (strain $\times 10^{-6}$). Strain measurement errors are more likely in the range of ± 10 microstrains.

HDP load distributions were generated for strain deviations of $\pm 0, 1, 2, \ldots, 10$ microstrains. The standard deviations of the x, y, and z loads for each strain deviation are plotted in Fig. 6. The x loads are twice as sensitive to strain deviations as either the y or the z loads. However, on a relative basis, the z loads are approximately twice as sensitive to strain variations as the y loads, and four times more sensitive than the x loads, as shown in Table 2.

The reason the x loads are most sensitive (on an absolute basis) to strain variations is the strains produced by a unit x load are approximately half the strains produced by either y or z loads, as shown in the next section.

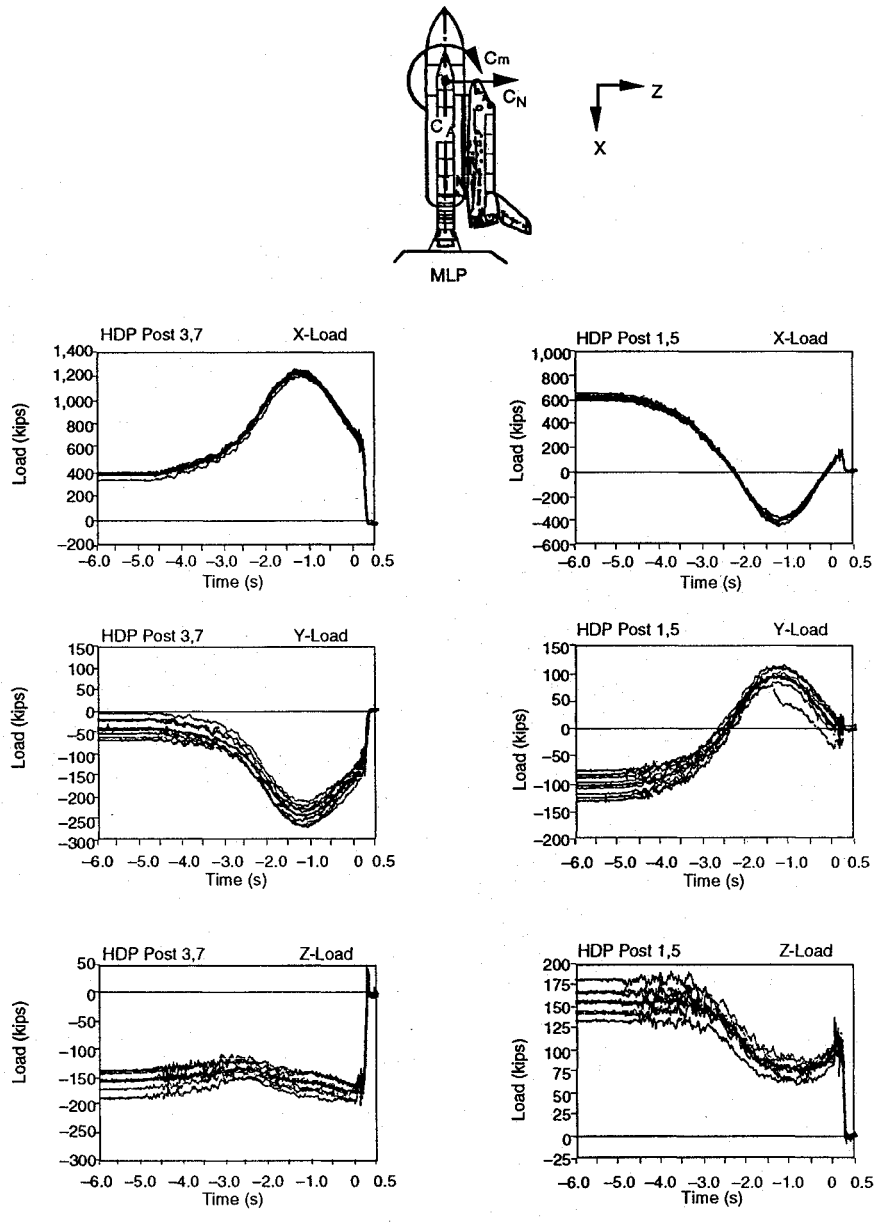

Fig. 3 HDP load histories.

Effect of Calibration Constant Variations on HDP Loads

The HDPs were calibrated by mounting each post in a test rig and applying measured loads in one direction only. Typical strain measurements at each of the eight gauges from a calibration procedure are shown in Table 3. These strains are the calibration constants for one HDP. The 8×3 matrix of calibration constants A was manipulated to produce the calibration matrix C as follows:

$$C = [A^T A]^{-1} A^T \tag{1}$$

The calibration matrix C multiplied by the strain measurements equals the HDP loads.

To study the sensitivity of the HDP loads to deviations in individual calibration constants, a single calibration constant was allowed to vary within ± 0.01 of its mean, while the other calibration constants remained constant. The calibration matrix C was then calculated and multiplied by the mean strains from Table 1. The procedure was repeated for each of the 24 calibration constants in Table 3. The results, presented in Fig. 7, show that not only the x loads, but also the y- and z loads, are most affected by variations in the x calibration constants. This implies that insensitivity to one load direction affects the sensitivity to the other load directions for this load cell. The average strain magnitude of the x-load calibration constants are approximately half the average strain magnitude of the y- and z-load calibration constants.

The effect on HDP loads of simultaneous variations in strain measurements and variations in calibration constants was studied by performing three sets of simulation runs. In the first set, the calibration constant deviations were set equal to zero. In the second set, the calibration constant deviation were set equal to their minimum values based on the results of the calibration tests. In the third set, the calibration constant deviations were set equal to higher but still realistic values. Uniform probability distributions were used to model the calibration constant variation.

An example showing the calibration constant deviations from a test on a single HDP is shown in Fig. 9. A total of 14 tests were completed for each strain gauge to determined the X calibration constants. The tests included both $+X$ and $-X$ axial loading with the HDP oriented in six different horizontal positions relative to the test fixture base. Each test configuration requires that the HDP be unbolted from the pedestal, reoriented, and then rebolted. Data scatter are attributed to slight differences in the position of the HDP relative to the test fixture pedestal (attributable to bolt–hole tolerances between the post and the pedestal). Also, data scatter occurred during the $+X$ and $-X$ axial load tests of a given configuration. In this case, data scatter results from slightly different load paths be-

Table 1 Base values for HDP loads and strains for eight-gauge model

Mean loads		Mean strains	
Load component	Load kips	Gauge no.	Strain, microstrains
Px	1,238	1	−84.6
Py	391	2	−136.0
Pz	−163	3	−239.2
		4	−276.8
		5	−191.6
		6	−108.0
		7	+48.2
		8	−39.4

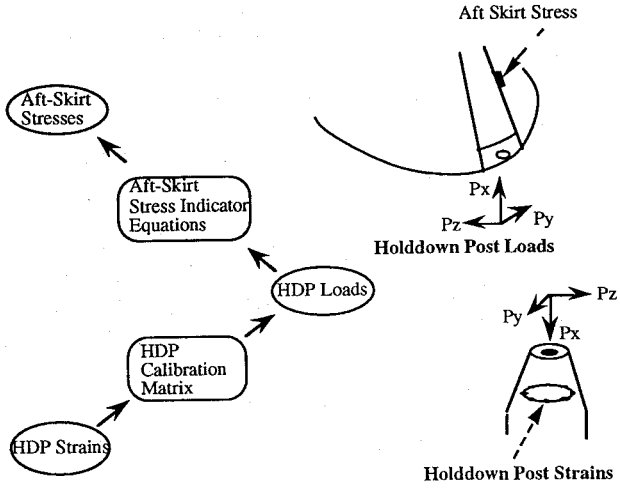

Fig. 4 Procedure for calculating aft-skirt stresses from measured HDP strains.

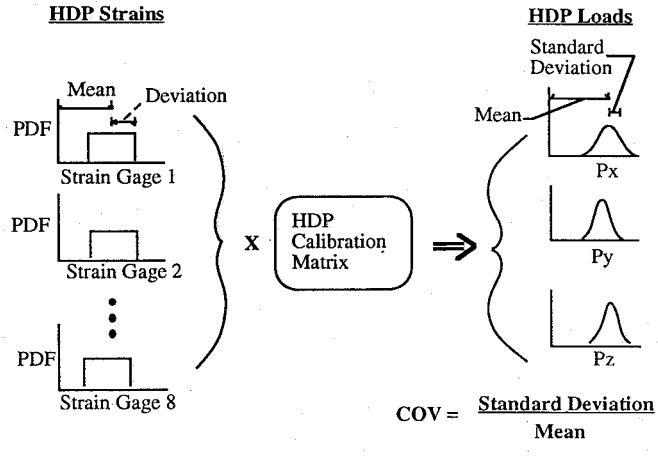

Fig. 5 Procedure for calculating HDP load distributions from HDP strain distributions.

tween tension $-X$ and compression $+X$ loading. Tension loads react from the bottom of the stud/post nut interface, whereas compression loads react into the post through the spherical bearing (Fig. 1). The X calibration factor was determined by averaging the 14 test values to give a single deterministic value. The Y and Z calibration constants were determined in a similar manner as X, but fewer tests per configuration were examined.

In the STS flight configuration, the HDP is bolted to a similar pedestal mounted on the MLP. Because the HDPs were calibrated independent of the MLP pedestal and then bolted into position, the "true" calibration constants for a given post are slightly different from those determined during the calibration tests. Based on abundant calibration data, as well as the extensive personal experience of the coauthor, the deviations listed in Table 4 were chosen for the minimum and the high calibration constant deviations.

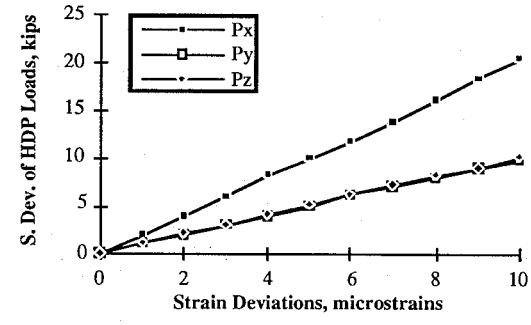

Fig. 6 Effect of strain deviation on X, Y, and Z HDP load deviations.

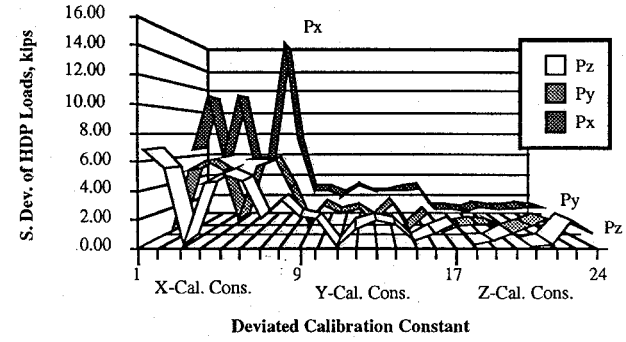

Fig. 7 Sensitivity of HDP loads to individual calibration constant deviations of ±0.01.

The results of the 33 simulation runs are shown in Fig. 8. In this figure, the standard deviations of the HDP loads are plotted separately but to the same scale for the x, y, and z loads. As expected, the x loads are more affected by the calibration constant deviations than either the y or z loads. The figure also shows that strain deviations have little effect when calibration constant deviations exist.

Effect of HDP Load Deviations on Aft-Skirt Stresses

The trends have been identified for the effect of strain and calibration constant deviations on HDP load deviations. The implications for the predicted aft-skirt stresses were investigated by constructing two representative sets of load distributions. For the first set (load case 1), minimum strain and calibration constant deviations were used. Higher but realistic strain and calibration constant deviations were used to construct the second set of load distributions (load case 2). The strain and calibration constant deviations for each load case are listed in the first column of Table 5. The resulting load distributions are plotted in Fig. 10; their standard deviations and COV are listed in Table 5.

The procedure for calculating aft-skirt stresses from HDP loads is shown in Fig. 11. The aft skirt is supported on four HDPs, each having an x, y, and z load component. The 12 HDP loads are premultiplied by a 4×12 matrix of stress indicator coefficients to yield four stresses. Each stress is located in the critical weld region above a HDP. Typical peak HDP loads during the buildup of the main engine were used as the mean values for the load distributions. The loads are listed in Table 6.

The stress indicator coefficients used to calculate the stress above HDP No. 8 (for the left skirt) are listed as follows. Stress above HDP No. 8 are equal to

$$\begin{aligned} &-0.650P_x^5 + 0.324P_y^5 + 0.921P_z^5 \\ &-0.420P_x^6 + 0.350P_y^6 + 1.414P_z^6 \\ &+1.900P_x^7 - 3.139P_y^7 + 3.037P_z^7 \\ &-11.00P_x^8 - 5.556P_y^8 - 27.62P_z^8 \end{aligned} \tag{2}$$

The subscripts denote the direction of the load and the superscripts denote the HDP number (the left skirt is supported on post numbers 5–8). Note that the predicted skirt stress is most sensitive to the z load of post 8.

Table 2 *X*, *Y*, and *Z* HDP load deviations vs strain deviations

Strain deviation microstrains	*Px* SD, kips	*Px* Absolute COV, %	*Py* SD, kips	*Py* Absolute COV, %	*Pz* SD, kips	*Pz* Absolute COV, %
0	0	0	0	0	0	0
2	3.9710	0.32	1.9240	0.49	1.9570	1.20
4	7.9770	0.64	3.9710	1.02	3.9660	2.44
6	12.1500	0.98	5.9560	1.52	5.9020	3.63
8	16.3500	1.32	8.0050	2.05	8.1140	4.99
10	19.7700	1.60	10.0700	2.58	10.2500	6.30

Table 3 HDP calibration constants

Strain gauge	Unit strains, microstrains/kip *X*-direction	*Y*-direction	*Z*-direction
1	−0.1023	+0.0585	−0.3220
2	−0.1041	−0.1829	−0.2032
3	−0.0836	−0.2813	+0.0538
4	−0.1147	−0.2881	+0.2558
5	−0.0927	−0.0080	+0.2401
6	−0.0952	+0.2029	+0.1607
7	−0.1055	+0.2502	+0.0292
8	−0.1063	+0.2076	−0.2023

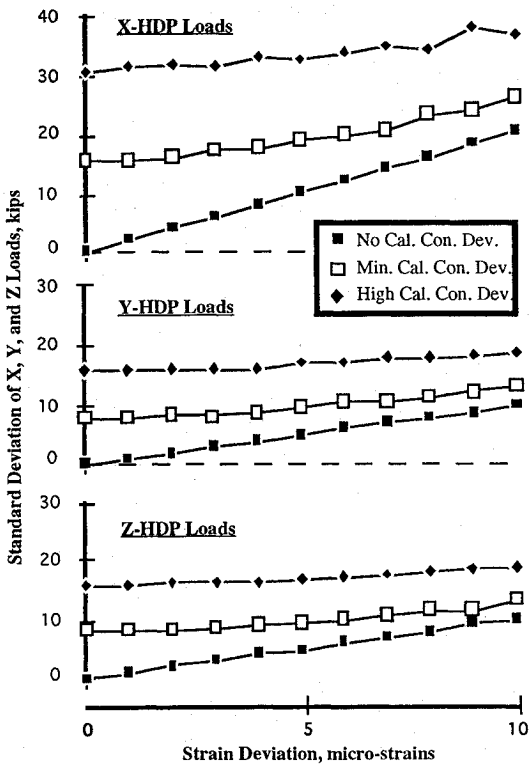

Fig. 8 Test results for *X*, *Y*, and *Z* calibration constants for a single HDP.

The results from the two simulation runs (shown in Fig. 12) indicate that, even with the minimum strain and calibration constant deviations, the predicted aft-skirt stresses are scattered over a 12-kips per square inch (ksi) range, where a kip is 1000 lb. When the strain and calibration deviations are doubled, the predicted skirt stresses are scattered over a 24-ksi range. The bar chart in Fig. 13 identifies the *x*-load deviation as the greatest contributor to the scatter in the predicted skirt stress. Figure 7 supports this finding. The uncertainty in the skirt weld stress is verified using the flight measured data plotted in Fig. 14.

Figure 14 graphs the predicted aft-skirt stresses vs the measured skirt strains in the critical weld region. The predicted stress values are based on the measured HDP loads and critical weld stress

Table 4 Calibration constant deviations used for simulation runs

	X-load constants	*Y*-load constants	*Z*-load constants
Minimum	±0.005	±0.01	±0.01
High	±0.01	±0.02	±0.02

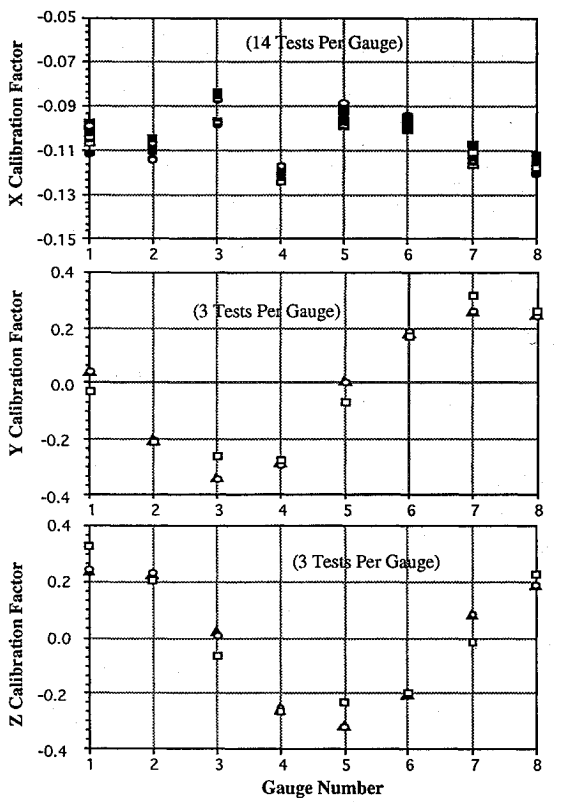

Fig. 9 Effect of calibration constant deviations and strain deviations on *x*-, *y*-, and *z*-direction HDP load deviations.

indicator (CWSI) equations [Eq. (2)]. Data from 18 Space Shuttle flights are plotted, as well as critical strains for compression posts 3, 4, 7, and 8. The data values correspond to aft-skirt weld peak stresses and strains at 1.2 s, just prior to liftoff. The dashed curve defines the expected relationship between the aft-skirt compression post strains and the critical weld stress. This curve was determined from a detailed math model of the skirt and verified through full-scale testing. Note that, for a given strain value, the critical weld stress predicted values are much higher than expected. If the skirt critical weld stress equation is assumed to be accurate, and the measured strain values define minimum uncertainty, then the load predictions must be in error.

Two types of errors are noted in Fig. 14. First, the offset distance between the expected and actual median stress curves indicates a gross measurement error in the loads (corresponding to about 15 ksi). It is believed that this result is caused by a moment load at the MLP post spherical bearing/aft-skirt shoe interface (both the math model and the test verification method assumed a zero interface moment). Second, scatter in the predicted skirt stress data about the

Table 5 Two HDP load distributions

Strain deviation, microstrains	Px SD, kips	Px Absolute COV, %	Py SD, kips	Py Absolute COV, %	Pz SD kips	Pz Absolute COV %
Load case 1 minimum errors	18.6	1.5	9.4	2.4	9.4	5.8
Strain deviation = ±5 u-strains X CC[a] = ±0.005 Y CC = ±0.01 Z CC = ±0.01						
Load case 2, high errors	38.6	3.1	19.0	4.9	19.2	11.9
Strain deviation = ±10 u-strains X CC = ±0.01 Y CC = ±0.02 Z CC = ±0.02						

[a]CC = Calibration constant deviation.

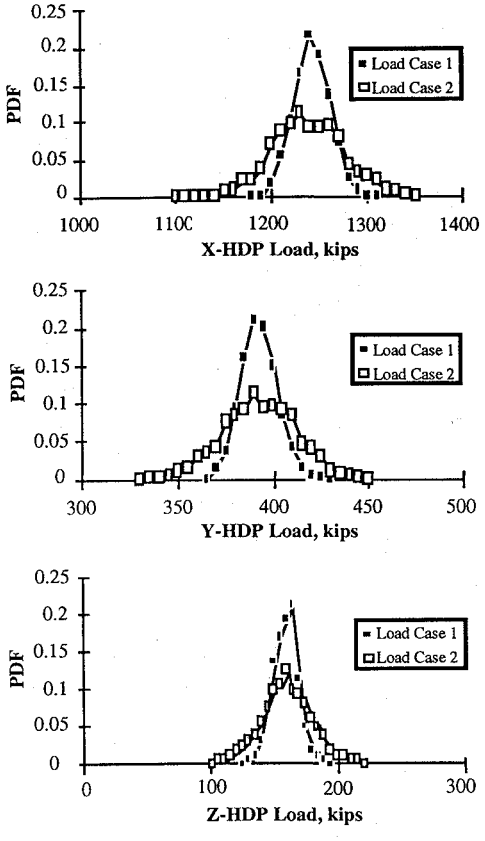

Fig. 10 Distributions of HDP loads for two cases.

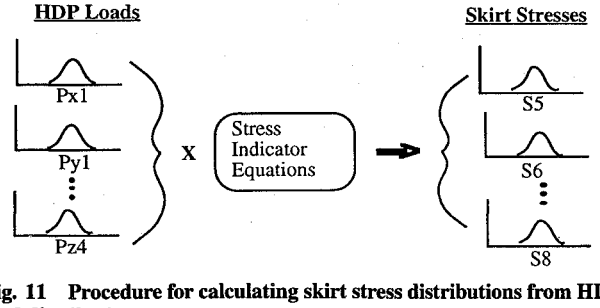

Fig. 11 Procedure for calculating skirt stress distributions from HDP load distributions.

Table 6 HDP mean loads used to calculated skirt stress distributions

HDP	Load direction	Mean load, kips
5	X	−440
	Y	51
	Z	61
6	X	−440
	Y	−100
	Z	88
7	X	1,120
	Y	−260
	Z	−300
8	X	1,310
	Y	285
	Z	−215

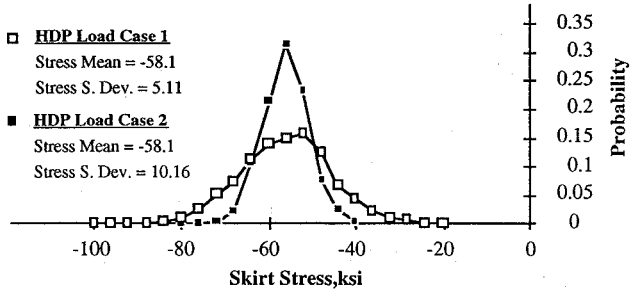

Fig. 12 Skirt stress distributions for two cases of strain and calibration constant deviations.

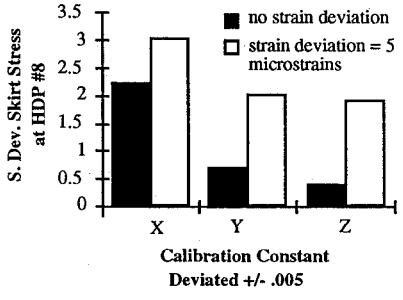

Fig. 13 Relative effect of calibration constant deviations on skirt stress above HDP no. 8.

actual median curve is similar to the data scatter identified previously in Fig. 12. This result implies that the uncertainty in the measured loads is caused in part by strain measurement error and calibration constant error.

The findings indicate that the measured HDP loads cannot predict aft-skirt stresses reliably. The principal reason behind the inadequacy of the load cells is the errors in the x-calibration constants (second column of Table 3). Errors in the x-calibration constants affect not only x-load predictions, but y and z loads as well. The x-calibration constants are susceptible to errors because they are small numbers.

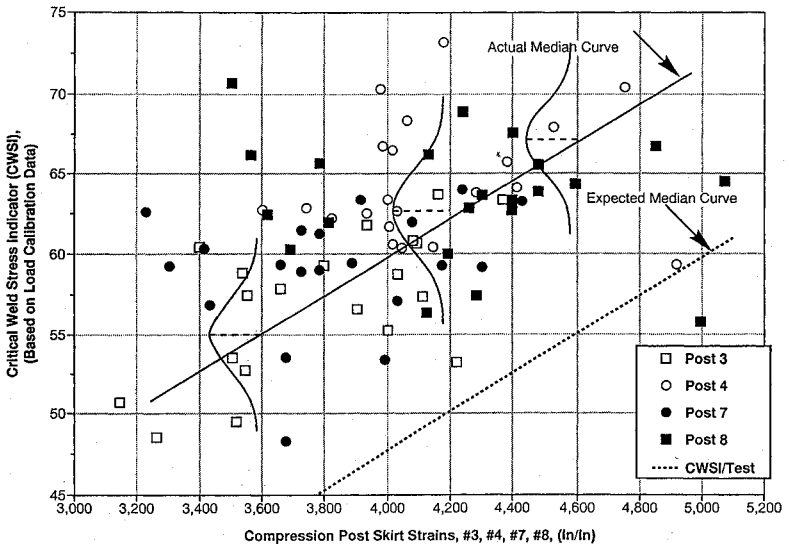

Fig. 14 STS flight measured skirt strains vs CWSI based on HDP load calibration (18 flights).

Conclusions

1) Simulation studies indicate that the instrumented HDPs are sensitive to small strain deviations and to typical calibration constant deviations. The minimum load deviations are approximately ±35 kips for x loads and ±20 kips for y and z loads. (These numbers represent ± two standard deviations.) Higher but not unrealistic load deviations are approximately ±70 kips for x loads and ±40 kips for y and z loads.

2) During calibration, the x-load strains are smaller than the strains caused by equal magnitude y or z loads. These smaller x-load strains are more susceptible to deviations (errors) in strain measurements and calibration procedures. When used as calibration constants, the x-load strains affect the dispersion of not only the x loads, but of the y and z loads as well.

3) The dispersion in the HDP loads causes deviations in the predicted aft-skirt stresses. Minimum deviation of the predicted skirt stresses is approximately ±6 ksi (± two standard deviations), whereas higher but realistic stress deviation is approximately ±14 ksi.

4) Finally, this study shown that probabilistic analysis can be used to evaluate the sensitivity of instrumentation to measurement errors. When used during design of the instrumentation, probabilistic analysis can improve the accuracy and reliability of future measurements.

Reference

[1]Richardson, J. A., and Townsend, J. S., "Characterizing the Uncertainty in Holddown Post Load Measurements," NASA TP 3332, March 1993.